

Tsunamigenic potential of a Holocene submarine landslide along the North Anatolian Fault (North Aegean Sea, off Thasos Island): insights from numerical modeling

Alexandre JANIN ¹, Mathieu RODRIGUEZ ¹, Dimitris SAKELLARIOU ², Vasilis LYKOUSIS ², and Christian GORINI ³

¹Laboratoire de Géologie de l'École normale supérieure de Paris; PSL research university, CNRS UMR 8538, 24 rue Lhomond, 75005 Paris, France.

²Institute of Oceanography, Hellenic Center of Marine Research, GR-19013 Anavyssos, Greece

³Sorbonne Universités, UPMC Université Paris 06, UMR 7193, IStEP, F-75005, Paris, France.

Correspondence to: Alexandre JANIN (alexandre.janin@ens.fr)

Abstract. The North Anatolian Fault in the northern Aegean Sea triggers frequent earthquakes of magnitude up to $M_w \sim 7$. This seismicity can be a source of modest tsunamis for the surrounding coastlines with less than 50 cm height according to numerical modelling and analysis of tsunami deposits. However, other tsunami sources may be involved, like submarine landslides. We assess the severity of this potential hazard by performing numerical simulations of tsunami generation and propagation from a Holocene landslide (1.85 km³ in volume) identified off Thasos island. We use a model coupling the simulation of the submarine landslide, assimilated to a granular flow, to the propagation of the tsunami wave. The results of these simulations show that a tsunami wave of water height between 1.10 m and 1.65 m reaches the coastline at Alexandroupolis (58.000 inhabitants) one hour after the triggering of the landslide. In the same way, tsunamis waves of water height between 0.80 m and 2.00 m reach the coastline of the Athos peninsula 9 min after the triggering of the landslide. Despite numerous earthquakes of $M_w > 7$ and strong detrital input (on the order of 30 cm.ka⁻¹), only a few Holocene landslides have been recognized so far, asking for tsunami recurrence in this area.

1 Introduction

Tsunamis constitute a major natural hazard for coastal populations and infrastructures. Tsunamis result from an impulsive perturbation of the seafloor, which generates waves with a wavelength $\lambda \sim 100$ km and a period in the 10 – 30 min range. According to the shallow-water approximation, the phase velocity of tsunami waves is expressed by $c = \sqrt{gh}$ at long period, where h is the bathymetry and g the gravitational acceleration. Although most of the deadliest tsunamis in the last decades result from earthquakes nucleated along submarine faults (Okal, 2015), other sources of damaging tsunamis have been identified, including submarine landslides (Tappin et al., 2008; ten Brink et al., 2014). One of the most conspicuous case-study is the July 1998 event that stroke the coastline of Papua-New Guinea. There, a $M_w \sim 7$ earthquake triggered a ~ 4 km³ submarine landslide offshore the Sissano Bay. The slide motion generated a tsunami with run-up values locally > 10 m, which caused more than 2200 casualties (Heinrich et al., 2000, 2001; Tappin et al., 2001, 2008). In the wake of the 1998 Sissano event, numerous

studies investigated the distribution of submarine landslides along continental slopes, islands and bathymetric highs, as well as their tsunamigenic potential (Canals et al., 2004; Masson et al., 2006; McAdoo et al., 2000; Chaytor et al., 2009; Twichell et al., 2009; Mulder et al., 2009; Tappin, 2010; Iacono et al., 2014; Urgeles and Camerlenghi, 2013; Macías et al., 2015; Palomino et al., 2016; Rodriguez et al., 2012, 2013, 2017; Katz et al., 2015). Submarine landslide-generated tsunamis display specific characteristics compared to other sources (Trifunac and Todorovska, 2002; Harbitz et al., 2006, 2014). Vertical displacements induced by the slide can be larger than displacements caused by earthquake related on-fault sea floor rupture and thus may produce higher wave amplitudes (Okal and Synolakis, 2003). Landslide motion can last over several minutes to hours, leading to complex patterns of wave interactions that either amplify or attenuate the wave amplitude (Haugen et al., 2005; Harbitz et al., 2006; Ma et al., 2013; Løvholt et al., 2015). For landslide volumes on the order of a few km³, frequency dispersion of the tsunami results in shorter wavelength and faster wave amplitude attenuation, and limits the far-field propagation of the tsunami.

Tsunami hazard along submarine strike-slip faults remains poorly investigated. Indeed, earthquakes along strike-slip faults generate only minor vertical displacement of the seafloor, and hence, minor tsunami, amplitude on the order of a few centimeters. However, releasing or restraining bends with steep slopes may take place along strike-slip faults, promoting submarine failures. For instance, the M_w 6.9 Loma Pietra earthquake along the San Andreas Fault excited tsunami up to 40 cm high in the Monterey Bay, which required a landslide as a secondary source (Ma et al., 1991). The lack of investigation of submarine landslides along submarine strike-slip fault may therefore result in under estimation of tsunami hazard in some places.

The North Anatolian Fault (Fig. 11) is a major, ~ 1200 -km-long continental strike-slip boundary, which is taking up the dextral relative motion between Anatolia and Eurasia at a current rate of ~ 25 mm.yr⁻¹ (Reilinger et al., 2006, 2010; Perouse et al., 2012; Müller et al., 2013). In the north Aegean domain the rate decreases from 21.2 mm.yr⁻¹ at the Saros Gulf to 7 mm.yr⁻¹ at the Sporades archipelago (Müller et al., 2013). The North Anatolian Fault is one of the most active fault system in Europe with several earthquakes above $M_w \sim 7$ recorded from instrumental seismology in the last decades, among which the deadly Izmit and Duzce events in 1999 (Hubert-Ferrari et al., 2000; Bulut et al., 2018). Detailed historical (Altinok et al., 2011) and field studies (Meghraoui et al., 2012) additionally revealed the geological signature of numerous past Holocene earthquakes and tsunamis. In the Marmara Sea, the response of sedimentary systems to the seismic activity has been investigated throughout detailed stratigraphic comparisons between the timing of mass wasting events and the timing of earthquakes (McHugh et al., 2006; Beck et al., 2007; Drab et al., 2012, 2015). Multibeam and seismic reflection data revealed the signature of numerous submarine landslides (Grall et al., 2012, 2013), among which some may have triggered tsunamis including the AD. 1509 event (Hébert et al., 2005; Özeren et al., 2010; Alpar et al., 2001; Yalçiner et al., 2002).

Although numerous tsunami deposits have been identified in the geological record along the northern aegean coastlines (Reicherter et al., 2010; Papadopoulos et al., 2014; Mathes-Schmidt et al., 2009) and despite the numerous cities along the coastline, the tsunamigenic potential of submarine landslides in this area remains only preliminary investigated (Karambas et al., 2012). The North Aegean Trough is a strike-slip basin emplaced along the North Anatolian Fault. Its tectono-sedimentary context is very similar to the Marmara Sea with splays of the North Anatolian Fault triggering frequent earthquakes up to $M_w \sim 7$ (such as the 24th May 2014 M_w 6.9 event in the Gulf of Saros) and with locally gas-charged sediments (Papatheodorou

et al., 1993). However, only one conspicuous submarine landslide has been identified so far along the edges of the North Aegean Trough (Lykousis et al., 2002). This submarine landslide emplaced at $40^{\circ} 15' N$, $24^{\circ} 52' E$, off Thasos Island, somewhere between 5500 and 7500 – 8500 years ago, and removed several km^3 of sediments (Lykousis et al., 2002). The slide was triggered at 300-m-depth, less than 50-km away from the surrounding coastlines, i.e. a configuration very similar to the 1998 Sissano event in Papua-New Guinea. For simplicity, this landslide is hereafter referred to as Thasos landslide. The objective of this paper is to investigate whether the Thasos landslide could have been a potential source of tsunami along the Aegean coasts by the mean of numerical modeling of tsunami generation and propagation. A particular emphasis is put on the possible wave interactions related to the complex morphology of the Aegean coastlines, with numerous islands, bays and peninsulas (Fig. 11). We adopt a deterministic approach based on the evaluation of credible scenarios defined and validated on the basis of the similarity between the observed and the modeled landslide extent.

2 Geological background of the Northern Aegean Sea and description of the Thasos submarine landslide

2.1 Tectonics and Morphology

The geological history of the Aegean Sea takes place in the complex realm of the collision between Africa and Eurasia during the Cenozoic. The Aegean domain used to be a mountain belt (Hellenides) during the Early Cenozoic, which collapsed since the Late Eocene-Early Oligocene, in close relationship with the southwards retreat of the Hellenic trench (Jolivet and Faccenna, 2000; Jolivet and Brun, 2010; Jolivet et al., 2013, 2015; Brun et al., 2016). Since the Late Miocene, strike-slip tectonics along the North Anatolian Fault system accommodates the lateral escape of Anatolia (Armijo et al., 1999; Faccenna et al., 2006; Hubert-Ferrari et al., 2009; Le Pichon et al., 2015; Bulut et al., 2018; Sakellariou and Tsampouraki-Kraounaki, 2018; Ferentinos et al., 2018). In the North Aegean Sea, the North Anatolian Fault system is divided into two main strike-slip systems, shaping the morphology of the seafloor. The age of inception of these strike-slip segments is estimated in the Plio-Pleistocene from ties of a vintage seismic dataset with industrial wells (Beniest et al., 2016).

The first, main fault segment to the north runs along the Saros Gulf, where it forms an en-échelon, negative flower structure system that connects the North Aegean Trough (Fig. 11) (Kurt et al., 2000; McNeill et al., 2004). This segment accommodates dextral shearing at a $\sim 20 \text{ mm.yr}^{-1}$ rate (Le Pichon and Kreemer, 2010; Perouse et al., 2012). It corresponds to the prolongation of the Main Marmara Fault (Roussos and Lyssimachou, 1991; Le Pichon et al., 2001) west of the Dardanelles Strait (Fig. 11). Numerous oblique NW-SE to E-W splays connects the North Anatolian Fault and form a horsetail structure, typical of strike-slip fault terminations. The horsetail structure forms a $\sim 150\text{-km-long}$, $\sim 60\text{-km-wide}$, $\sim 1500 \text{ m-deep}$ basin, referred as the North Aegean Trough (Papanikolaou et al., 2002; Sakellariou and Tsampouraki-Kraounaki, 2016; Sakellariou et al., 2016), where the oblique splays isolate a series of half-grabens, tilted over a crustal detachment at $\sim 10\text{-km-depth}$ (Laigle et al., 2000). This complex structural pattern results in a very uneven bathymetry, with a series of bathymetric highs and lows within the North Aegean Trough. Southwards, the second strike-slip splay corresponds to the southern branch of the North Anatolian Fault, active at a $\sim 5 \text{ mm.yr}^{-1}$ rate (Le Pichon and Kreemer, 2010; Le Pichon et al., 2014). This structure ends off Skyros Island, where it forms the Edremit Trough (Fig. 11).

2.2 Sedimentology

During the Quaternary, the deposition of detritic sediments coming from the surrounding lands (Suc et al., 2015) has been controlled by fast subsidence (0.3 to 1.5 m.Kyrs⁻¹) (Piper and Perissoratis, 1991) and glacio-eustatic variations of sea-level (İşler et al., 2008). In the vicinity of the North Aegean Trough, the Late Quaternary (i.e. last 150 kyrs) sediments are composed of pro-delta formations, composed of sandy to silty turbidites (Piper and Perissoratis, 1991; Lykousis et al., 2002). The uppermost sediments (2 m below seafloor) consist in normally consolidated or slightly over-consolidated muddy to silty sediments, with a bulk density of sediments ranging between 1.4 and 1.5 g.cm⁻³ (Lykousis et al., 2002).

2.3 The Holocene Thasos submarine landslide

On the bathymetry, the slide of around 30-km-long scar encloses an area of 85-km². Downslope, a 75 – m-thick lobe-shape deposit spans an area of ~ 50 km² (Fig. 12(a,b))(Lykousis et al., 2002). The mass transport deposit is characterized by a hummocky facies on the seafloor and displays a typical facies composed of chaotic and hyperbolic reflectors on the seismic profiles (Unit 2, in orange on Fig. 12(b,c)). A second 5-m-thick minor mass transport deposit spreads around the failure plan over 8.7-km from the top the scarp (Unit 1, in red on Fig. 12(b,c)). The initial volume, mobilized during the first step of the failure, is estimated following the method described in Ten Brink et al. (2006). It consists in filling-in the failed area according to the adjacent scar height. The difference between the filled-in grid and the grid displaying the slide scar gives an initial failed volume at 1.85 km³ in the case of the Thasos slide. The volume of the lobe-shaped mass transport deposit lying at the bottom of the scar is estimated at ~ 3.8 km³ (Lykousis et al., 2002). The difference between the initial failed volume and the final volume of the slide means that during its flow, the slide has captured sediments from the adjacent slope. The slide evolved as a translational slide of well-bedded sediments, over a glide plane corresponding to a muddy weak layer deposited 170 – 245 kyrs ago (Lykousis et al., 2002). Although earthquake shaking related to the activity of the North Anatolian Fault may be considered as the most likely trigger of submarine landslides, recent $M_w \sim 7$ events did not trigger significant landslides and tsunami, despite the unstable state of the North Aegean Trough slopes (Lykousis et al., 2002). This discrepancy between strong earthquakes and landslide frequencies has been highlighted in various tectono-sedimentary contexts (Völker et al., 2011; Strozyk et al., 2010; Pope et al., 2015, 2016). Various process may explain this discrepancy, including the amount and the nature of sedimentary supply, local variations in physical properties of the sediments (Lafuerza et al., 2012) or the over-compaction of the sediments subsequent to the fluid release induced by the seismic wave shaking (Hampton et al., 1996; Strozyk et al., 2010). Some mass transport deposits, probably older than Holocene, can be guessed on sparker lines in the Sporadhes basin (Brooks and Ferentinos, 1980; Ferentinos et al., 1981; Sakellariou et al., 2018; Rodriguez et al., 2018) and on sub-bottom profiles crossing the Saros Gulf (McNeill et al., 2004). However, a comprehensive map of the spatial distribution of landslides and precise stratigraphic constraints on their recurrence are lacking to further describe how the sedimentary system reacts to the seismic activity of the North Anatolian Fault.

3 Numerical modeling of the submarine landslide and the associated tsunami

3.1 Bathymetric dataset

The bathymetric grid used for tsunami calculations is a compilation of several grids of different resolutions. We use the multi-beam grid previously published in Papanikolaou et al. (2002), acquired with a seabeam 2120 working at 20 kHz. The horizontal resolution is ~ 100 m, for a vertical resolution on the order of 1 m. At the slide location, we include the high-resolution (30-m horizontal resolution) grid acquired by HCMR in 2013-2015 onboard the Aegeo, in the frame of the YPOTHER project (Sakellariou et al., 2016). The remaining gaps have been filled-in with the SRTM PLUS bathymetry (Becker et al., 2009).

3.2 Slide modeling: physical background and limits

We use the AVALANCHE code that has been successfully tested from comparisons with tidal measurements for the 1998 Papua New Guinea tsunami (Heinrich et al., 2000) and the 1979 Nice event (Labbé et al., 2012). Two approaches are commonly used to model the dynamics of a submarine landslide. A first approach assimilates the slide to a viscous flow, with a Bingham rheology. The slide is divided into a bottom layer submitted to shear along the glide plane, and a top plug layer with a uniform velocity profile (Jiang and LeBlond, 1993). This approach efficiently reproduced some landslides in the Mediterranean Sea (Iglesias et al., 2012; Løvholt et al., 2015). However, in our case, all the simulations carried for a reasonable range of dynamic viscosities ($25 - 500 \text{ m}^2 \cdot \text{s}^{-1}$) failed to reproduce the first-order morphology of the Thasos slide, and lead to excessive runout and volume values. The second approach, which assimilates the propagation of the landslide to a granular flow (Savage and Hutter, 1989), produced more convincing results in our case, which may be consistent with the detritic nature of the sediments off Thasos (Piper and Perissoratis, 1991; Lykousis et al., 2002). Modelling the slide as a granular flow implies the sediment loses its cohesion immediately after failure occurred at the glide plane. This model assumes that the energy dissipated at the glide plane is much higher than the energy dissipated within the sedimentary flow itself. Although large deformations throughout the thickness of the flow are inevitable (ten Brink et al., 2014) and may have important effects on the evolution of the tsunami wave (Ma et al., 2013), the configuration of the slide (thickness smaller than its length and its width) allows the use of the shallow water assumption (Savage and Hutter, 1989), and therefore the simplification of the mechanical behavior within the sedimentary flow. Deformations within the flow in the earliest stages of collapse are also neglected, as well as the added mass effect (Løvholt et al., 2015), which may result in slightly overestimated initial acceleration (on the order of $10^{-2} \text{ m} \cdot \text{s}^{-2}$). The velocity of the flow in the direction parallel to the slope is considered constant over the entire thickness of the slide. Basal friction at the glide plane is modeled by a Coulomb-type friction law (Savage and Hutter, 1989). This law assumes a constant ratio of the shear stress to the normal stress at the base of the slide and involves a dynamic friction angle ϕ between the rough bed and the sliding mass. Granular flows commonly occur for internal friction angles (ϕ) around $30 - 40^\circ$. However, this range of values is not appropriate for submarine landslides, which involve ϕ values $< 15^\circ$ (Canals et al., 2004; Ten Brink et al., 2009), and even ϕ values $< 2^\circ$ for low slope gradient (Rodriguez et al., 2012; Urlaub et al., 2015). Therefore, we perform simulations only for friction angles ranging between 1 and 5° to simulate the Thasos landslide, which spans the range of slope

values in this area. The nonlinear and nondispersive equations from shallow water assumption, written in a coordinate system linked to the topography, give us (Heinrich et al., 2000):

fluid mass conservation:

$$\frac{\partial h}{\partial t} + \frac{\partial}{\partial x}(hu) + \frac{\partial}{\partial y}(hv) = e_w(u + v) \quad (1)$$

5 momentum conservation equations:

$$\frac{\partial}{\partial t}(hu) + \alpha \frac{\partial}{\partial x}(hu \cdot u) + \alpha \frac{\partial}{\partial y}(hu \cdot v) = -\frac{1}{2}\kappa \frac{\partial}{\partial x}(gh^2 \cos \theta) + \kappa gh \sin \theta_x - \tau_{xz(z=0)} \quad (2)$$

$$\frac{\partial}{\partial t}(hv) + \alpha \frac{\partial}{\partial x}(hv \cdot u) + \alpha \frac{\partial}{\partial y}(hv \cdot v) = -\frac{1}{2}\kappa \frac{\partial}{\partial y}(gh^2 \cos \theta) + \kappa gh \sin \theta_y - \tau_{yz(z=0)} \quad (3)$$

sediment mass conservation:

$$10 \quad \frac{\partial}{\partial t}(ch) + \frac{\partial}{\partial x}(chu) + \frac{\partial}{\partial y}(chv) = 0 \quad (4)$$

where:

- $h(x, y, t)$ the thickness of the landslide perpendicular to the glide plane
- \mathbf{u} the velocity vector with its components (u, v) in accordance with x and y axis, respectively
- $\kappa = 1 - \rho_w / \rho_s$ with ρ_s the sediment density; $\rho_s = 1450 \text{ kg.m}^{-3}$ according to in-situ measurements (Lykousis et al., 2002) and ρ_w , the water density. Here we consider $\rho_w = 1000 \text{ kg.m}^{-3}$
- c the sediment concentration at a mean depth
- $\theta(x, y)$ the local sliding angle with θ_x, θ_y respectively its components in accordance with x and y axis
- $\tau_{xz(z=0)}$ and $\tau_{yz(z=0)}$ are the shear stresses at the bed surface. The constitutive law governing granular flows is generally the Coulomb-type friction law defined in the x-direction by : $\tau_{xz(z=0)} = \kappa gh \cos \theta \tan \phi \frac{u}{\|\mathbf{u}\|}$
- 20 - e_w the water entrainment coefficient ($e_w \in [0, 0.01]$) (Fukushima et al., 1985; Kostic and Parker, 2006; Sequeiros et al., 2009). It corresponds to the dilution of the sedimentary mass by water incorporation at the interface between the slide and the water.
- α is a parameter characterizing the deviation of the velocity profile compared to a homogeneous distribution profile. Modelling landslide as a granular flow requires a linear profile and $\alpha = 4/3$ (Heinrich et al., 2001).

25 The main limit of the simulation of a past submarine landslide is the impossibility to provide constraints on the pattern of velocity and acceleration of the slide from the geological record (Harbitz et al., 2006; Ma et al., 2013; Løvholt et al., 2015). We therefore consider scenarios where slide velocities are compatible with the few constraints available from submarine cable breaks recorded in the 20th century i.e., with mean velocity $< 20 - 30 \text{ m.s}^{-1}$ and initial acceleration $< 0.6 \text{ m.s}^{-2}$ (Heezen and Ewing, 1952; Mulder et al., 1997; Fine et al., 2005).

3.3 Tsunami modeling

Simulations of the tsunami waves are also based on the shallow-water approximation, which deals with the full interaction of landslide and water, including the deformation of the sediment body. Equations governing the landslide and the tsunami propagation are similar and are thus solved using the same Godunov-type scheme, extended to second order by using the concept of Vanleer (Alcrudo and Garcia-Navarro, 1993; Mangeney et al., 2000). This model is particularly adapted to nonlinear waves. The time history of sea bottom deformation resulting from the landslide is introduced as a known forcing term $(\cos \theta)^{-1} \partial h / \partial t$ in the mass conservation equation of the tsunami model (Heinrich et al., 2000).

4 Results

4.1 Elaboration of Landslide and Tsunami Scenarios

We simulate the tsunami that would be triggered in the present-day context by a slide similar to the Thasos slide. Credible scenarios are defined according to the range of parameters able to reproduce as closely as possible the first-order morphology of the observed mass transport deposit (i.e. fitting the following criteria: area of the deposit, volume, runout). Credible scenarios (Table. 11) are obtained for a range of basal friction angle ϕ between $1.5 - 1.8^\circ$ and an initial volume of failure of 1.85 km^3 (Fig. 13). The selection of the most credible scenarios is buttressed on the basis of normalized inverse distance weighting (Shepard, 1968) (Appendix A).

4.2 Propagation of the Tsunami potentially generated by the Thasos landslide

For each selected scenario, we present maps of tsunami propagation at different, representative time steps (10, 16, 28 and 43 minutes ; Fig. 14, Fig. 17). We also plot maps of the maximal water heights reached after a 2 h propagation time in the entire study area (Fig. 15, Fig. 18), which helps to identify bathymetric forcing effect on the tsunami elevation. The propagation of the tsunami at the source displays the same pattern in every scenario, typical of landslide generated tsunami (Ward, 2001; Mohammed and Fritz, 2012; Ma et al., 2013). At the source, the incipient radiated wave has two peaks and one trough (Fig. 14). The water ahead of the front face of the slide (i.e. the out-going wave) is pushed away, creating a leading positive wave in the slide direction (i.e. towards the Chalkidiki Peninsula and the Thermaikos Gulf). The trough following the crest is simultaneously created by the slide excavation, and is followed by a large second positive peak created by the infilling of the trough. In contrast, the front of the wave propagating in the opposite direction of the slide (i.e. the back-going wave) forms a trough propagating towards Alexandroupolis, followed by a second positive wave (Fig. 14). Among the 40 simulations carried out, we present two of them where the deposit is well reproduced, but leading to different tsunami elevation (Table. 12).

4.2.1 First scenario

The first scenario is obtained for a basal friction angle ϕ of 1° and a water entrainment coefficient of 10^{-3} . Although the runout of the modeled slide is slightly overestimated by $\sim 2 \text{ km}$, the modeled volume is 3.7 km^3 , which compares closely

to the observations (Fig. 13). The thickness of the modeled deposit, between 20 and 40 m, is also in fair agreement with the observations from the seismic line crossing the Thasos slide (Fig. 13). In this scenario, the maximal velocity of the slide reaches the value of 30 m.s^{-1} about 6 minutes after the slide beginning. During this phase, the acceleration of the slide is on the order of 0.2 m.s^{-2} . We describe the propagation of the tsunami following the timing of arrival of the leading wave at the coastline.

5 At the source, the slide generates a tsunami with a maximal water elevation at 3.6 m (Fig. 15). After 8 minutes of propagation, the leading out-going wave reaches the Chalkidiki Peninsula and the island of Lemnos, with local amplification up to 1.25 m. The front of the out-going wave then sweeps the coast of the Athos Peninsula towards the Orfani Gulf. There, the leading wave reaches an elevation up to 1.20 m-high after ~ 40 minutes of propagation (Fig. 14). The tsunami then propagates into the multiple gulf formed by the 'finger-like' pattern of the Chalkidiki Peninsula (Fig. 14). The tsunami enters the Sigitikos Gulf

10 after ~ 15 minutes of propagation, then the Kassandra Gulf after ~ 28 minutes of propagation and eventually the Thermaikos Gulf after ~ 40 minutes of propagation. Tsunami elevation reaches 0.8 – 0.9 m in the Sigitikos Gulf, but remains below 0.4-m in the Kassandra Gulf (Fig. 14). The coastline running from the Sporades to the Thermaikos Gulf is stroke by a ~ 0.5 -m-high tsunami (Fig. 14). A bathymetric through related to a splay of the North Aegean Trough off Kassandra Peninsula is responsible of the focalization and the amplification of the tsunami before it enters the Thermaikos Gulf (Fig. 14). South of the source,

15 the leading out-going wave reaches the North of Lemnos after ~ 10 minutes of propagation and Agios Efstratios island at $t = 26$ min (Fig. 14), where complex phenomenons of wave interactions lead to tsunami elevation on the order of 1.4 m at the coastline. The leading back-going wave is split in several fronts propagating at different speeds when it reaches the Samothraki and Gokceada Islands after ~ 16 minutes of propagation. A 1.65-m-high tsunami strikes Alexandroupolis after 1h07min of propagation (Fig. 14). The complex pattern of the Aegean coastline results in a complex pattern of wave interactions that either

20 destroy or amplify the tsunami (Fig. 16). Amplification through resonance is expected within the Sigitikos Bay, the Orfani Gulf, and the Pournias Bay north of Lemnos (Fig. 14). South East of Agios Efstratios and north of Samothraki, we observe lineaments where the tsunami wave is amplified (on the order of 50 cm), despite the lack of bathymetric feature that could explain local forcing. Constructive interferences between the waves that surrounded these islands may produce this amplification. At both locations, the leading wave is split in two wave fronts that rotate along the islands by a coastal attraction phenomenon, until the

25 two wave fronts merge together, leading to wave amplification. For instance, the back-going wave of the tsunami is split in two wave fronts when it strikes Samothraki at $t = 28$ min (Fig. 16). After their propagation around the island, both fronts collide at $t = 36$ min, which results in constructive interferences that amplify the wave up to $\sim 0.5 - 0.6$ m. A second positive wave front, which has been amplified along the Thracian coast (Fig. 16 at 43 min), collides with the back-going wave front formed east of Samothraki. This interference cancels the negative polarity of the back-going wave, and even amplifies the tsunami

30 front up to 1.65 m at Alexandroupolis.

4.2.2 Second scenario

The second selected scenario is obtained for a basal friction angle ϕ of 1.5° and a water entrainment coefficient e_w of 5.10^{-4} . In this model, the area of the mass transport deposit is larger than the observations, resulting in an overestimated but still reasonable volume of 4.1 km^3 (Fig. 13). In this case, the maximal velocity of the slide reaches 25 m.s^{-1} about 3 minutes

5
6
7
8
9
10
11
12
13
14
15
16
17
18
19
20
21
22
23
24
25
26
27
28
29
30
31
32
33
34
35
36
37
38
39
40
41
42
43
44
45
46
47
48
49
50
51
52
53
54
55
56
57
58
59
60
61
62
63
64
65
66
67
68
69
70
71
72
73
74
75
76
77
78
79
80
81
82
83
84
85
86
87
88
89
90
91
92
93
94
95
96
97
98
99
100
101
102
103
104
105
106
107
108
109
110
111
112
113
114
115
116
117
118
119
120
121
122
123
124
125
126
127
128
129
130
131
132
133
134
135
136
137
138
139
140
141
142
143
144
145
146
147
148
149
150
151
152
153
154
155
156
157
158
159
160
161
162
163
164
165
166
167
168
169
170
171
172
173
174
175
176
177
178
179
180
181
182
183
184
185
186
187
188
189
190
191
192
193
194
195
196
197
198
199
200
201
202
203
204
205
206
207
208
209
210
211
212
213
214
215
216
217
218
219
220
221
222
223
224
225
226
227
228
229
230
231
232
233
234
235
236
237
238
239
240
241
242
243
244
245
246
247
248
249
250
251
252
253
254
255
256
257
258
259
260
261
262
263
264
265
266
267
268
269
270
271
272
273
274
275
276
277
278
279
280
281
282
283
284
285
286
287
288
289
290
291
292
293
294
295
296
297
298
299
300
301
302
303
304
305
306
307
308
309
310
311
312
313
314
315
316
317
318
319
320
321
322
323
324
325
326
327
328
329
330
331
332
333
334
335
336
337
338
339
340
341
342
343
344
345
346
347
348
349
350
351
352
353
354
355
356
357
358
359
360
361
362
363
364
365
366
367
368
369
370
371
372
373
374
375
376
377
378
379
380
381
382
383
384
385
386
387
388
389
390
391
392
393
394
395
396
397
398
399
400
401
402
403
404
405
406
407
408
409
410
411
412
413
414
415
416
417
418
419
420
421
422
423
424
425
426
427
428
429
430
431
432
433
434
435
436
437
438
439
440
441
442
443
444
445
446
447
448
449
450
451
452
453
454
455
456
457
458
459
460
461
462
463
464
465
466
467
468
469
470
471
472
473
474
475
476
477
478
479
480
481
482
483
484
485
486
487
488
489
490
491
492
493
494
495
496
497
498
499
500
501
502
503
504
505
506
507
508
509
510
511
512
513
514
515
516
517
518
519
520
521
522
523
524
525
526
527
528
529
530
531
532
533
534
535
536
537
538
539
540
541
542
543
544
545
546
547
548
549
550
551
552
553
554
555
556
557
558
559
560
561
562
563
564
565
566
567
568
569
570
571
572
573
574
575
576
577
578
579
580
581
582
583
584
585
586
587
588
589
590
591
592
593
594
595
596
597
598
599
600
601
602
603
604
605
606
607
608
609
610
611
612
613
614
615
616
617
618
619
620
621
622
623
624
625
626
627
628
629
630
631
632
633
634
635
636
637
638
639
640
641
642
643
644
645
646
647
648
649
650
651
652
653
654
655
656
657
658
659
660
661
662
663
664
665
666
667
668
669
670
671
672
673
674
675
676
677
678
679
680
681
682
683
684
685
686
687
688
689
690
691
692
693
694
695
696
697
698
699
700
701
702
703
704
705
706
707
708
709
710
711
712
713
714
715
716
717
718
719
720
721
722
723
724
725
726
727
728
729
730
731
732
733
734
735
736
737
738
739
740
741
742
743
744
745
746
747
748
749
750
751
752
753
754
755
756
757
758
759
760
761
762
763
764
765
766
767
768
769
770
771
772
773
774
775
776
777
778
779
780
781
782
783
784
785
786
787
788
789
790
791
792
793
794
795
796
797
798
799
800
801
802
803
804
805
806
807
808
809
810
811
812
813
814
815
816
817
818
819
820
821
822
823
824
825
826
827
828
829
830
831
832
833
834
835
836
837
838
839
840
841
842
843
844
845
846
847
848
849
850
851
852
853
854
855
856
857
858
859
860
861
862
863
864
865
866
867
868
869
870
871
872
873
874
875
876
877
878
879
880
881
882
883
884
885
886
887
888
889
890
891
892
893
894
895
896
897
898
899
900
901
902
903
904
905
906
907
908
909
910
911
912
913
914
915
916
917
918
919
920
921
922
923
924
925
926
927
928
929
930
931
932
933
934
935
936
937
938
939
940
941
942
943
944
945
946
947
948
949
950
951
952
953
954
955
956
957
958
959
960
961
962
963
964
965
966
967
968
969
970
971
972
973
974
975
976
977
978
979
980
981
982
983
984
985
986
987
988
989
990
991
992
993
994
995
996
997
998
999
1000

after the slide triggering. During this phase, the slide acceleration is on the order of $\sim 0.15 \text{ m.s}^{-2}$. This second scenario leads to the same timing and mode of propagation of the tsunami, with similar processes of wave amplifications and interactions around the islands of Agios Efstratios and Samothraki (Fig. 17). However, the tsunami elevation is less important everywhere. The maximum of water elevation is reduced at $\sim 85 \text{ cm}$ along the Chalkidiki Peninsula, at $\sim 1.10 \text{ m}$ at Alexandroupolis, and around 50 cm at Agios Efstratios and north of Lemnos. Amplification within the bay of Sigitikos, Kassandra, and the Gulf of Thermaikos is also reduced, with water heights less than 20 cm (Fig. 18).

5 Discussion

Our simulations were able to strikingly reproduce the first-order morphological characteristics of the Thassos slide, using basic granular flow behaviour governed by a simple Coulomb friction law at the glide plane. Therefore, the selected range of physical parameters used for the granular flow modeling, and the resulting tsunami, are considered realistic. Compared to previous studies (Karambas et al., 2012), the advantage of our approach is the coupling between the dynamic of the slide, the formation of the tsunami and its propagation.

The results of our simulations show that the Thassos slide has probably been tsunamigenic. If a similar slide occurs at the current sea level, the areas of Alexandroupolis (57812 inhabitant in 2011 according to the Hellenic Statistical Authority), the Chalkidiki Peninsula and Agios Efstratios would be the most threatened, with tsunami elevations at the coastline ranging between 1 and 2 m according to the model parameters.

The Tsunami strikes most of the coastlines of the northern Aegean Sea after less than 1 hour of propagation (Table. 12). The Athos Peninsula is reached after just 10 minutes, but is not densely populated and the topography does not allow large run up distances. The geomorphological context of the Thassos Slide is similar to slide at the origin of the Papua-New Guinea tsunami in 1998 (roughly the same volume, slope, and distance to the coastline), but the numerous interactions between waves due to the numerous bays and islands makes the expected high of the tsunami at the Aegean coastline lower. The tsunami simulations have some limits. The first one is the lack of high-resolution bathymetry along the coast, which does not allow accurate computation of the flooding onland. It remains unknown if local bathymetric features or harbors would result in further amplification or dispersion of the tsunami wave. This is especially critical for the numerous gulf (Orfani, Sigitikos and Kassandra) where resonance is expected. Run-up values being often more important than the water height calculated a few kilometers from the coastline (Synolakis, 1987), the computed tsunami elevations at the coastline should be considered as minimum values of the actual run up. Moreover, the initial slide acceleration and its speed strongly impinge on the initial pattern of the tsunami, including the pattern of short wavelengths, and therefore on the subsequent frequency dispersion (Haugen et al., 2005). Even if the modeled values of slide velocity and acceleration fit with values measured on slides triggered in the 20th-21st centuries (Heezen and Ewing, 1952; Mulder et al., 1997; Pope et al., 2016), geological records are not sufficient to determine these parameters for Holocene period.

A second-order source of simplification is the non-dispersive numerical model that is not able to account for frequency dispersion inherent in tsunamis with short wavelengths. However, the density of the mobilized sediments is quite low ($\sim 1500 \text{ kg.m}^{-3}$). Frequency dispersion at the source is expected to be negligible for this range of densities (Ma et al., 2013).

6 Conclusion

- 5 The results of our simulations show that the expected tsunami wave from the Thasos slide are higher (165 cm for Alexandroupolis or 145 cm for the costs of Agios Efstratios, Sporades Archipelago and Athos Peninsula) than values expected in the case of an earthquake along the North Anatolian Fault, and higher than run up values (between 20 and 50 cm south of Thessaloniki) documented from tsunami deposits in the Thermaikos Gulf (Reicherter et al., 2010). The study highlights the need to build a comprehensive map of the distribution of landslides within the North Aegean Trough, as well as a full quantification of their volumes, to better estimate the variety of tsunami scenarios in the area . This discrepancy between earthquake and land-slide recurrence asks the question of the response of sedimentary systems to ground shaking. The tsunami hazard related to submarine landslides similar to Thassos is less severe than tsunami associated to landslides triggered during the 1956 Amorgos event (Perissoratis and Papadopoulos, 1999; Okal et al., 2009); or tsunami triggered during or subsequent to volcanic events (e.g. Santorini in the Bronze age (Novikova et al., 2011).

15 Appendix A: Selection of Tsunami scenario

In order to quantify the gap between landslide simulation results and data from bathymetry and seismic profiles we used an 'normalized inverse distance weighting' function. Thereby we define a weight function ω as:

$$\omega = \sum_{k=1}^4 \frac{1}{d_k(x_k, x_k^{th})^p} \quad (\text{A1})$$

Where:

- 20 – x_k are parameters used for determined the differences between the numerical simulation and the bathymetry. We used for x_k : (1) the sliding direction, (2) the total surface of deposit, (3) the amplitude of the discontinuity in the thickness of sediments between units 1 and 2 (Fig. 12) and (4) the final volume of the deposit.
- x_k^{th} are the used observable parameters from the bathymetry and the seismic profiles corresponding to x_k
- $d_k(x_k, x_k^{th})$ are distance functions between x_k and x_k^{th} . We define here d_k as $d_k = |x_k^{th} - x_k|$
- 25 – p is a real positive number, called the power parameter. If $p > 1$, the contribution in ω of the small distance is amplified (we used here $p = 1$).

The higher the ω , the closer the scenario is to bathymetry and seismic data. The function ω is calculated for all scenarios and allows us to highlight the two scenarios presented in this study. The computation of ω for the 2 credible scenarios gives $\omega = 181.52$ and $\omega = 2.56$ (Fig. 13)

Acknowledgements. We acknowledge the support of the "Yves Rocard" Joint Laboratory between the École Normale Supérieure, the Commissariat à l'Énergie Atomique, and the CNRS.

References

- Alcrudo, F. and Garcia-Navarro, P.: A high-resolution Godunov-type scheme in finite volumes for the 2D shallow-water equations, *International Journal for Numerical Methods in Fluids*, 16, 489–505, 1993.
- Alpar, B., Yalciner, A. C., Imamura, F., and Synolakis, C. E.: Determination of probable underwater failures and modeling of tsunami
5 propagation in the Sea of Marmara, in: *Proceedings of the International Tsunami Symposium ITS*, pp. 535–544, 2001.
- Altinok, Y., Alpar, B., Özer, N., and Aykurt, H.: Revision of the tsunami catalogue affecting Turkish coasts and surrounding regions, *Natural Hazards and Earth System Sciences*, 11, 273, 2011.
- Armijo, R., Meyer, B., Hubert, A., and Barka, A.: Westward propagation of the North Anatolian fault into the northern Aegean: Timing and kinematics, *Geology*, 27, 267–270, 1999.
- 10 Beck, C., de Lépinay, B. M., Schneider, J.-L., Cremer, M., Çağatay, N., Wendenbaum, E., Boutareaud, S., Ménot, G., Schmidt, S., Weber, O., et al.: Late Quaternary co-seismic sedimentation in the Sea of Marmara's deep basins, *Sedimentary Geology*, 199, 65–89, 2007.
- Becker, J., Sandwell, D., Smith, W., Braud, J., Binder, B., Depner, J., Fabre, D., Factor, J., Ingalls, S., Kim, S., et al.: Global bathymetry and elevation data at 30 arc seconds resolution: SRTM30_PLUS, *Marine Geodesy*, 32, 355–371, 2009.
- Beniest, A., Brun, J.-P., Gorini, C., Crombez, V., Deschamps, R., Hamon, Y., and Smit, J.: Interaction between trench retreat and anatolian
15 escape as recorded by neogene basins in the northern Aegean Sea, *Marine and Petroleum Geology*, 77, 30–42, 2016.
- Brooks, M. and Ferentinos, G.: Structure and evolution of the Sporadhes basin of the North Aegean trough, northern Aegean Sea, *Tectonophysics*, 68, 15–30, 1980.
- Brun, J.-P., Faccenna, C., Gueydan, F., Sokoutis, D., Philippon, M., Kydonakis, K., and Gorini, C.: The two-stage Aegean extension, from localized to distributed, a result of slab rollback acceleration, *Canadian journal of earth sciences*, 53, 1142–1157, 2016.
- 20 Bulut, F., Özener, H., Doğru, A., Aktuğ, B., and Yaltrak, C.: Structural setting along the Western North Anatolian Fault and its influence on the 2014 North Aegean Earthquake (Mw 6.9), *Tectonophysics*, 2018.
- Canals, M., Lastras, G., Urgeles, R., Casamor, J., Mienert, J., Cattaneo, A., De Batist, M., Haffidason, H., Imbo, Y., Laberg, J., et al.: Slope failure dynamics and impacts from seafloor and shallow sub-seafloor geophysical data: case studies from the COSTA project, *Marine Geology*, 213, 9–72, 2004.
- 25 Chaytor, J. D., Uri, S., Solow, A. R., and Andrews, B. D.: Size distribution of submarine landslides along the US Atlantic margin, *Marine Geology*, 264, 16–27, 2009.
- Drab, L., Hubert, A., Schmidt, S., and Martinez, P.: The earthquake sedimentary record in the western part of the Sea of Marmara, Turkey, *Natural Hazards & Earth System Sciences*, 2012.
- Drab, L., Hubert-Ferrari, A., Schmidt, S., Martinez, P., Carlut, J., and El Ouahabi, M.: Submarine earthquake history of the Çınarcık segment
30 of the North Anatolian Fault in the Marmara Sea, Turkey, *Bulletin of the Seismological Society of America*, 105, 622–645, 2015.
- Faccenna, C., Bellier, O., Martinod, J., Piromallo, C., and Regard, V.: Slab detachment beneath eastern Anatolia: A possible cause for the formation of the North Anatolian fault, *Earth and Planetary Science Letters*, 242, 85–97, 2006.
- Ferentinos, G., Brooks, M., and Collins, M.: Gravity-induced deformation on the north flank and floor of the Sporadhes Basin of the North Aegean Sea Trough, *Marine Geology*, 44, 289–302, 1981.
- 35 Ferentinos, G., Georgiou, N., Christodoulou, D., Geraga, M., and Papatheodorou, G.: Propagation and termination of a strike slip fault in an extensional domain: The westward growth of the North Anatolian Fault into the Aegean Sea, *Tectonophysics*, 2018.

- Fine, I., Rabinovich, A., Bornhold, B., Thomson, R., and Kulikov, E.: The Grand Banks landslide-generated tsunami of November 18, 1929: preliminary analysis and numerical modeling, *Marine Geology*, 215, 45–57, 2005.
- Fritz, H. M., Phillips, D. A., Okayasu, A., Shimozone, T., Liu, H., Mohammed, F., Skanavis, V., Synolakis, C. E., and Takahashi, T.: The 2011 Japan tsunami current velocity measurements from survivor videos at Kesenuma Bay using LiDAR, *Geophysical Research Letters*, 5 39, 2012.
- Fukushima, Y., Parker, G., and Pantin, H.: Prediction of ignitive turbidity currents in Scripps Submarine Canyon, *Marine Geology*, 67, 55–81, 1985.
- Grall, C., Henry, P., Tezcan, D., de Lpinay, B. M., Bécel, A., Géli, L., Rudkiewicz, J.-L., Zitter, T., and Harmegnies, F.: Heat flow in the Sea of Marmara Central Basin: Possible implications for the tectonic evolution of the North Anatolian fault, *Geology*, 40, 3–6, 2012.
- 10 Grall, C., Henry, P., Thomas, Y., Westbrook, G., Çağatay, M., Marsset, B., Saritas, H., Çifçi, G., and Geli, L.: Slip rate estimation along the western segment of the Main Marmara Fault over the last 405–490 ka by correlating mass transport deposits, *Tectonics*, 32, 1587–1601, 2013.
- Hampton, M. A., Lee, H. J., and Locat, J.: Submarine landslides, *Reviews of geophysics*, 34, 33–59, 1996.
- Harbitz, C. B., Løvholt, F., Pedersen, G., and Masson, D. G.: Mechanisms of tsunami generation by submarine landslides: a short review., 15 *Norwegian Journal of Geology/Norsk Geologisk Forening*, 86, 2006.
- Harbitz, C. B., Løvholt, F., and Bungum, H.: Submarine landslide tsunamis: how extreme and how likely?, *Natural Hazards*, 72, 1341–1374, 2014.
- Haugen, K. B., Løvholt, F., and Harbitz, C. B.: Fundamental mechanisms for tsunami generation by submarine mass flows in idealised geometries, *Marine and Petroleum Geology*, 22, 209–217, 2005.
- 20 Hébert, H., Schindele, F., Altinok, Y., Alpar, B., and Gazioglu, C.: Tsunami hazard in the Marmara Sea (Turkey): a numerical approach to discuss active faulting and impact on the Istanbul coastal areas, *Marine Geology*, 215, 23–43, 2005.
- Heezen, B. C. and Ewing, M.: Turbidity currents and submarine slumps, and the 1929 Grand Banks earthquake, *American journal of Science*, 250, 849–873, 1952.
- Heinrich, P., Piatanesi, A., Okal, E., and Hébert, H.: Near-field modeling of the July 17, 1998 tsunami in Papua New Guinea, *Geophysical 25 Research Letters*, 27, 3037–3040, 2000.
- Heinrich, P., Piatanesi, A., and Hebert, H.: Numerical modelling of tsunami generation and propagation from submarine slumps: the 1998 Papua New Guinea event, *Geophysical Journal International*, 145, 97–111, 2001.
- Hubert-Ferrari, A., Barka, A., Jacques, E., Nalbant, S. S., et al.: Seismic hazard in the Marmara Sea region following the 17 August 1999 Izmit earthquake, *Nature*, 404, 269, 2000.
- 30 Hubert-Ferrari, A., King, G., Van Der Woerd, J., Villa, I., Altunel, E., and Armijo, R.: Long-term evolution of the North Anatolian Fault: new constraints from its eastern termination, *Geological Society, London, Special Publications*, 311, 133–154, 2009.
- Iacono, C. L., Gràcia, E., Ranero, C. R., Emelianov, M., Huvenne, V. A., Bartolomé, R., Booth-Rea, G., Prades, J., Ambroso, S., Dominguez, C., et al.: The West Melilla cold water coral mounds, Eastern Alboran Sea: Morphological characterization and environmental context, *Deep Sea Research Part II: Topical Studies in Oceanography*, 99, 316–326, 2014.
- 35 Iglesias, O., Lastras, G., Canals, M., Olabarrieta, M., Gonzalez, M., Aniel-Quiroga, Í., Otero, L., Duran, R., Amblas, D., Casamor, J. L., et al.: The BIG'95 submarine landslide-generated tsunami: a numerical simulation, *The Journal of Geology*, 120, 31–48, 2012.
- İşler, E., Aksu, A., Yaltrak, C., and Hiscott, R.: Seismic stratigraphy and Quaternary sedimentary history of the northeast Aegean Sea, *Marine Geology*, 254, 1–17, 2008.

- Jiang, L. and LeBlond, P. H.: Numerical modeling of an underwater Bingham plastic mudslide and the waves which it generates, *Journal of Geophysical Research: Oceans*, 98, 10 303–10 317, 1993.
- Jolivet, L. and Brun, J.-P.: Cenozoic geodynamic evolution of the Aegean, *International Journal of Earth Sciences*, 99, 109–138, 2010.
- Jolivet, L. and Faccenna, C.: Mediterranean extension and the Africa-Eurasia collision, *Tectonics*, 19, 1095–1106, 2000.
- 5 Jolivet, L., Faccenna, C., Huet, B., Labrousse, L., Le Pourhiet, L., Lacombe, O., Lecomte, E., Burov, E., Denele, Y., Brun, J.-P., et al.: Aegean tectonics: Strain localisation, slab tearing and trench retreat, *Tectonophysics*, 597, 1–33, 2013.
- Jolivet, L., Menant, A., Sternai, P., Rabillard, A., Arbaret, L., Augier, R., Laurent, V., Beaudoin, A., Grasemann, B., Huet, B., et al.: The geological signature of a slab tear below the Aegean, *Tectonophysics*, 659, 166–182, 2015.
- Karambas, T. V., Hasiotis, T., et al.: A Study of Tsunamis Generated by Underwater Landslides in the Aegean Sea, in: *The Twenty-second International Offshore and Polar Engineering Conference*, International Society of Offshore and Polar Engineers, 2012.
- 10 Katz, O., Reuven, E., and Aharonov, E.: Submarine landslides and fault scarps along the eastern Mediterranean Israeli continental-slope, *Marine Geology*, 369, 100–115, 2015.
- Kostic, S. and Parker, G.: The response of turbidity currents to a canyon–fan transition: internal hydraulic jumps and depositional signatures, *Journal of Hydraulic Research*, 44, 631–653, 2006.
- 15 Kurt, H., Demirbağ, E., and Kuşçu, İ.: Active submarine tectonism and formation of the Gulf of Saros, Northeast Aegean Sea, inferred from multi-channel seismic reflection data, *Marine Geology*, 165, 13–26, 2000.
- Labbé, M., Donnadiou, C., Daubord, C., and Hébert, H.: Refined numerical modeling of the 1979 tsunami in Nice (French Riviera): Comparison with coastal data, *Journal of Geophysical Research: Earth Surface*, 117, 2012.
- Lafuerza, S., Sultan, N., Canals, M., Lastras, G., Cattaneo, A., Frigola, J., Costa, S., and Berndt, C.: Failure mechanisms of Ana Slide from geotechnical evidence, Eivissa Channel, Western Mediterranean Sea, *Marine Geology*, 307, 1–21, 2012.
- 20 Laigle, M., Hirn, A., Sachpazi, M., and Roussos, N.: North Aegean crustal deformation: an active fault imaged to 10 km depth by reflection seismic data, *Geology*, 28, 71–74, 2000.
- Le Pichon, X. and Kreemer, C.: The Miocene-to-present kinematic evolution of the eastern Mediterranean and Middle East and its implications for dynamics, *Annual Review of Earth and Planetary Sciences*, 38, 323–351, 2010.
- 25 Le Pichon, X., Şengör, A., Demirbağ, E., Rangin, C., Imren, C., Armijo, R., Görür, N., Çağatay, N., De Lepinay, B. M., Meyer, B., et al.: The active main Marmara fault, *Earth and Planetary Science Letters*, 192, 595–616, 2001.
- Le Pichon, X., Imren, C., Rangin, C., Şengör, A. C., and Siyako, M.: The South Marmara Fault, *International Journal of Earth Sciences*, 103, 219–231, 2014.
- Le Pichon, X., Şengör, A. C., Kende, J., İmren, C., Henry, P., Grall, C., and Karabulut, H.: Propagation of a strike-slip plate boundary within an extensional environment: the westward propagation of the North Anatolian Fault, *Canadian Journal of Earth Sciences*, 53, 1416–1439, 2015.
- 30 Løvholt, F., Pedersen, G., Harbitz, C. B., Glimsdal, S., and Kim, J.: On the characteristics of landslide tsunamis, *Phil. Trans. R. Soc. A*, 373, 20140 376, 2015.
- Lykousis, V., Roussakis, G., Alexandri, M., Pavlakis, P., and Papoulia, I.: Sliding and regional slope stability in active margins: North Aegean Trough (Mediterranean), *Marine Geology*, 186, 281–298, 2002.
- 35 Ma, G., Kirby, J. T., and Shi, F.: Numerical simulation of tsunami waves generated by deformable submarine landslides, *Ocean Modelling*, 69, 146–165, 2013.

- Ma, K.-F., Satake, K., and Kanamori, H.: The origin of the tsunami excited by the 1989 Loma Prieta Earthquake—Faulting or slumping?, *Geophysical Research Letters*, 18, 637–640, 1991.
- Macías, J., Vázquez, J., Fernández-Salas, L., González-Vida, J., Bárcenas, P., Castro, M., Díaz-del Río, V., and Alonso, B.: The Al-Borani submarine landslide and associated tsunami. A modelling approach, *Marine Geology*, 361, 79–95, 2015.
- 5 Mangeney, A., Heinrich, P., and Roche, R.: Analytical solution for testing debris avalanche numerical models, *Pure and Applied Geophysics*, 157, 1081–1096, 2000.
- Masson, D., Harbitz, C., Wynn, R., Pedersen, G., and Løvholt, F.: Submarine landslides: processes, triggers and hazard prediction, *Philosophical Transactions of the Royal Society of London A: Mathematical, Physical and Engineering Sciences*, 364, 2009–2039, 2006.
- Mathes-Schmidt, M., Papanikolaou, J., and Reicherter, K.: Event deposits in the Eastern Thermaikos Gulf and Kassandra Peninsula (Northern Greece) and evidence of the 479 BC Herodotus-tsunami, *paleoseismicity.org*, 2009.
- 10 McAdoo, B., Pratson, L., and Orange, D.: Submarine landslide geomorphology, US continental slope, *Marine Geology*, 169, 103–136, 2000.
- McHugh, C. M., Seeber, L., Cormier, M.-H., Dutton, J., Çagatay, N., Polonia, A., Ryan, W. B., and Gorur, N.: Submarine earthquake geology along the North Anatolia Fault in the Marmara Sea, Turkey: a model for transform basin sedimentation, *Earth and Planetary Science Letters*, 248, 661–684, 2006.
- 15 McNeill, L., Mille, A., Minshull, T., Bull, J., Kenyon, N., and Ivanov, M.: Extension of the North Anatolian Fault into the North Aegean Trough: Evidence for transtension, strain partitioning, and analogues for Sea of Marmara basin models, *Tectonics*, 23, 2004.
- Meghraoui, M., Aksoy, M. E., Akyüz, H. S., Ferry, M., Dikbaş, A., and Altunel, E.: Paleoseismology of the North Anatolian fault at Güzelköy (Ganos segment, Turkey): Size and recurrence time of earthquake ruptures west of the Sea of Marmara, *Geochemistry, Geophysics, Geosystems*, 13, 2012.
- 20 Mohammed, F. and Fritz, H. M.: Physical modeling of tsunamis generated by three-dimensional deformable granular landslides, *Journal of Geophysical Research: Oceans*, 117, 2012.
- Mulder, T., Savoye, B., and Syvitski, J.: Numerical modelling of a mid-sized gravity flow: the 1979 Nice turbidity current (dynamics, processes, sediment budget and seafloor impact), *Sedimentology*, 44, 305–326, 1997.
- Mulder, T., Gonthier, E., Lecroart, P., Hanquiez, V., Marches, E., and Voisset, M.: Sediment failures and flows in the Gulf of Cadiz (eastern Atlantic), *Marine and Petroleum Geology*, 26, 660–672, 2009.
- 25 Müller, M., Geiger, A., Kahle, H.-G., Veis, G., Billiris, H., Paradissis, D., and Felekis, S.: Velocity and deformation fields in the North Aegean domain, Greece, and implications for fault kinematics, derived from GPS data 1993–2009, *Tectonophysics*, 597, 34–49, 2013.
- Novikova, T., Papadopoulos, G., and McCoy, F.: Modelling of tsunami generated by the giant late Bronze Age eruption of Thera, South Aegean Sea, Greece, *Geophysical Journal International*, 186, 665–680, 2011.
- 30 Okal, E. A.: The quest for wisdom: lessons from 17 tsunamis, 2004–2014, *Phil. Trans. R. Soc. A*, 373, 20140370, 2015.
- Okal, E. A. and Synolakis, C. E.: A theoretical comparison of tsunamis from dislocations and landslides, *Pure and Applied Geophysics*, 160, 2177–2188, 2003.
- Okal, E. A., Synolakis, C. E., Uslu, B., Kalligeris, N., and Voukouvalas, E.: The 1956 earthquake and tsunami in Amorgos, Greece, *Geophysical Journal International*, 178, 1533–1554, 2009.
- 35 Özeren, M. S., Çağatay, M. N., Postacıoğlu, N., Şengör, A. C., Görür, N., and Eriş, K.: Mathematical modelling of a potential tsunami associated with a late glacial submarine landslide in the Sea of Marmara, *Geo-Marine Letters*, 30, 523–539, 2010.

- Palomino, D., Vázquez, J.-T., Somoza, L., León, R., López-González, N., Medialdea, T., Fernández-Salas, L.-M., González, F.-J., and Rengel, J. A.: Geomorphological features in the southern Canary Island Volcanic Province: The importance of volcanic processes and massive slope instabilities associated with seamounts, *Geomorphology*, 255, 125–139, 2016.
- Papadopoulos, G. A., Gràcia, E., Urgeles, R., Sallares, V., De Martini, P. M., Pantosti, D., González, M., Yalciner, A. C., Mascle, J., Sakellariou, D., et al.: Historical and pre-historical tsunamis in the Mediterranean and its connected seas: Geological signatures, generation mechanisms and coastal impacts, *Marine Geology*, 354, 81–109, 2014.
- Papanikolaou, D., Alexandri, M., Nomikou, P., and Ballas, D.: Morphotectonic structure of the western part of the North Aegean Basin based on swath bathymetry, *Marine Geology*, 190, 465–492, 2002.
- Papatheodorou, G., Hasiotis, T., and Ferentinos, G.: Gas-charged sediments in the Aegean and Ionian Seas, Greece, *Marine Geology*, 112, 171–184, 1993.
- Perissoratis, C. and Papadopoulos, G.: Sediment instability and slumping in the southern Aegean Sea and the case history of the 1956 tsunami, *Marine Geology*, 161, 287–305, 1999.
- Perouse, E., Chamot-Rooke, N., Rabaute, A., Briole, P., Jouanne, F., Georgiev, I., and Dimitrov, D.: Bridging onshore and offshore present-day kinematics of central and eastern Mediterranean: implications for crustal dynamics and mantle flow, *Geochemistry, Geophysics, Geosystems*, 13, 2012.
- Piper, D. J. and Perissoratis, C.: Late Quaternary Sedimentation on the North Aegean Continental Margin, Greece (1), *AAPG bulletin*, 75, 46–61, 1991.
- Pope, E., Talling, P., Urlaub, M., Hunt, J., Clare, M., and Challenor, P.: Are large submarine landslides temporally random or do uncertainties in available age constraints make it impossible to tell?, *Marine Geology*, 369, 19–33, 2015.
- Pope, E. L., Talling, P. J., and Carter, L.: Which earthquakes trigger damaging submarine mass movements: Insights from a global record of submarine cable breaks?, *Marine Geology*, 384, 131–146, 2016.
- Reicherter, K., Papanikolaou, I., Roger, J., Mathes-Schmidt, M., Papanikolaou, D., Rössler, S., Grützner, C., and Stamatis, G.: Holocene tsunamigenic sediments and tsunami modelling in the Thermaikos Gulf area (northern Greece), *Zeitschrift für Geomorphologie, Supplementary Issues*, 54, 99–125, 2010.
- Reilinger, R., McClusky, S., Vernant, P., Lawrence, S., Ergintav, S., Cakmak, R., Ozener, H., Kadirov, F., Guliev, I., Stepanyan, R., et al.: GPS constraints on continental deformation in the Africa-Arabia-Eurasia continental collision zone and implications for the dynamics of plate interactions, *Journal of Geophysical Research: Solid Earth*, 111, 2006.
- Reilinger, R., McClusky, S., Paradissis, D., Ergintav, S., and Vernant, P.: Geodetic constraints on the tectonic evolution of the Aegean region and strain accumulation along the Hellenic subduction zone, *Tectonophysics*, 488, 22–30, 2010.
- Rodriguez, M., Fournier, M., Chamot-Rooke, N., Huchon, P., Zaragosi, S., and Rabaute, A.: Mass wasting processes along the Owen Ridge (northwest Indian Ocean), *Marine Geology*, 326, 80–100, 2012.
- Rodriguez, M., Chamot-Rooke, N., Hébert, H., Fournier, M., and Huchon, P.: Owen Ridge deep-water submarine landslides: implications for tsunami hazard along the Oman coast, *Natural Hazards and Earth System Sciences*, 13, 417–424, 2013.
- Rodriguez, M., Maleuvre, C., Jollivet-Castelot, M., d’Acremont, E., Rabaute, A., Lafosse, M., Ercilla, G., Vázquez, J.-T., Alonso, B., and Ammar, A.: Tsunamigenic submarine landslides along the Xauen–Tofiño banks in the Alboran Sea (Western Mediterranean Sea), *Geophysical Journal International*, 209, 266–281, 2017.

- Rodriguez, M., Sakellariou, D., Gorini, C., Chamot-Rooke, N., d'Acremont, E., Nercessian, A., Tsampouraki Kraounaki, K., Oregioni, D., Delescluse, M., and Janin, A.: Seismic profiles across the North Anatolian Fault in the Aegean Sea, in: EGU General Assembly Conference Abstracts, vol. 20, p. 7426, 2018.
- Roussos, N. and Lyssimachou, T.: Structure of the Central North Aegean Trough: an active strike-slip deformation zone, *Basin research*, 3, 39–48, 1991.
- Sakellariou, D. and Tsampouraki-Kraounaki, K.: Offshore faulting in the Aegean Sea: A synthesis based on bathymetric and seismic profiling data, *Bulletin of the Geological Society of Greece*, 50, 124–133, 2016.
- Sakellariou, D. and Tsampouraki-Kraounaki, K.: Plio-Quaternary Extension and Strike-Slip Tectonics in the Aegean, in: *Transform Plate Boundaries and Fracture Zones*, edited by Duarte, J., chap. 14, Elsevier, 2018.
- 10 Sakellariou, D., Rousakis, G., Vougioukalakis, G., Ioakim, C., Panagiotopoulos, I., Morfis, I., Zimianitis, E., Athanasoulis, K., Tsampouraki-Kraounaki, K., Mpardis, D., and Karageorgis, A.: Deformation pattern in the western North Aegean trough: preliminary results, *Bulletin of the Geological Society of Greece*, 50, 134–143, 2016.
- Sakellariou, D., Rousakis, G., Morfis, I., Panagiotopoulos, I., Ioakim, C., Trikalinou, G., Tsampouraki-Kraounaki, K., Kranis, H., and Karageorgis, A.: Deformation and kinematics at the termination of the North Anatolian Fault: the North Aegean Trough horsetail structure, 15 INQUA Focus Group Earthquake Geology and Seismic Hazards, paleoseismicity.org, 2018.
- Savage, S. B. and Hutter, K.: The motion of a finite mass of granular material down a rough incline, *Journal of fluid mechanics*, 199, 177–215, 1989.
- Sequeiros, O. E., Naruse, H., Endo, N., Garcia, M. H., and Parker, G.: Experimental study on self-accelerating turbidity currents, *Journal of Geophysical Research: Oceans*, 114, 2009.
- 20 Shepard, D.: A two-dimensional interpolation function for irregularly-spaced data, in: *Proceedings of the 1968 23rd ACM national conference*, pp. 517–524, ACM, 1968.
- Strozyk, F., Strasser, M., Förster, A., Kopf, A., and Huhn, K.: Slope failure repetition in active margin environments: constraints from submarine landslides in the Hellenic fore arc, eastern Mediterranean, *Journal of Geophysical Research: Solid Earth*, 115, 2010.
- Suc, J.-P., Popescu, S.-M., Do Couto, D., Clauzon, G., Rubino, J.-L., Melinte-Dobrinescu, M. C., Quillévéré, F., Brun, J.-P., Dumurdžanov, 25 N., Zagorchev, I., et al.: Marine gateway vs. fluvial stream within the Balkans from 6 to 5Ma, *Marine and Petroleum Geology*, 66, 231–245, 2015.
- Synolakis, C. E.: The runup of solitary waves, *Journal of Fluid Mechanics*, 185, 523–545, 1987.
- Tappin, D.: Submarine mass failures as tsunami sources: their climate control, *Philosophical Transactions of the Royal Society of London A: Mathematical, Physical and Engineering Sciences*, 368, 2417–2434, 2010.
- 30 Tappin, D., Watts, P., McMurtry, G., Lafoy, Y., and Matsumoto, T.: The Sissano, Papua New Guinea tsunami of July 1998—offshore evidence on the source mechanism, *Marine Geology*, 175, 1–23, 2001.
- Tappin, D., Watts, P., and Grilli, S.: The Papua New Guinea tsunami of 17 July 1998: anatomy of a catastrophic event, *Natural Hazards and Earth System Science*, 8, 243–266, 2008.
- Ten Brink, U., Barkan, R., Andrews, B. D., and Chaytor, J.: Size distributions and failure initiation of submarine and subaerial landslides, 35 *Earth and Planetary Science Letters*, 287, 31–42, 2009.
- Ten Brink, U. S., Geist, E. L., and Andrews, B. D.: Size distribution of submarine landslides and its implication to tsunami hazard in Puerto Rico, *Geophysical Research Letters*, 33, 2006.

- ten Brink, U. S., Chaytor, J. D., Geist, E. L., Brothers, D. S., and Andrews, B. D.: Assessment of tsunami hazard to the US Atlantic margin, *Marine Geology*, 353, 31–54, 2014.
- Trifunac, M. and Todorovska, M.: A note on differences in tsunami source parameters for submarine slides and earthquakes, *Soil Dynamics and Earthquake Engineering*, 22, 143–155, 2002.
- 5 Twichell, D. C., Chaytor, J. D., Uri, S., and Buczkowski, B.: Morphology of late Quaternary submarine landslides along the US Atlantic continental margin, *Marine Geology*, 264, 4–15, 2009.
- Urgeles, R. and Camerlenghi, A.: Submarine landslides of the Mediterranean Sea: Trigger mechanisms, dynamics, and frequency-magnitude distribution, *Journal of Geophysical Research: Earth Surface*, 118, 2600–2618, 2013.
- Urlaub, M., Talling, P. J., Zervos, A., and Masson, D.: What causes large submarine landslides on low gradient ($< 2^\circ$) continental slopes with
10 slow (0.15 m/kyr) sediment accumulation?, *Journal of Geophysical Research: Solid Earth*, 120, 6722–6739, 2015.
- Völker, D., Scholz, F., and Geersen, J.: Analysis of submarine landsliding in the rupture area of the 27 February 2010 Maule earthquake, Central Chile, *Marine Geology*, 288, 79–89, 2011.
- Ward, S. N.: Landslide tsunami, *Journal of Geophysical Research: Solid Earth*, 106, 11 201–11 215, 2001.
- Yalçiner, A. C., Alpar, B., Altınok, Y., Özbay, İ., and Imamura, F.: Tsunamis in the Sea of Marmara: Historical documents for the past,
15 models for the future, *Marine Geology*, 190, 445–463, 2002.

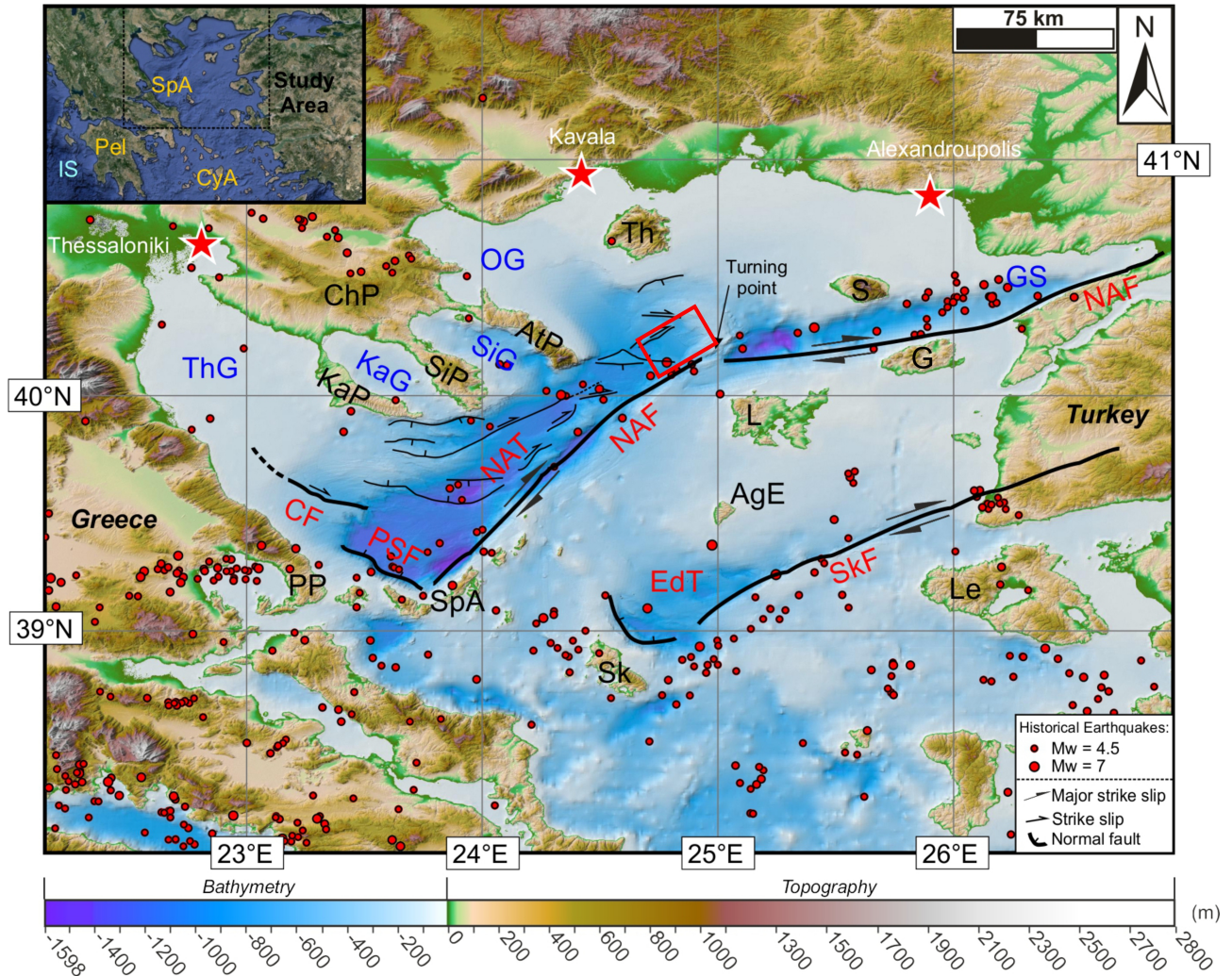


Figure 11. General morphological features of the studied area. The main fault are indicated (after Sakellariou and Tsampouraki-Kraounaki (2016)). Seismicity from USGS, since January 1st 1950, for earthquake with $M_w > 4.5$. The red rectangle gives the location of the Thasos landslide. In inset, location of the study area (background from Google Earth). AgE: Agios Efstratios, AS: Aegean Sea, AtP: Athos Peninsula, ChP: Chalkidiki Peninsula, CyA: Cyclades Archipelago, EdT: Edremit Trough, G: Gokceada (Imvros), GS: Gulf of Saros, IS: Ionian Sea, KaG: Kassandra Gulf, KaP: Kassandra Peninsula, L: Lemnos, Le: Lesvos, NAT: North Aegean Trough, NAF: North Anatolian Fault, OG: Orfani Gulf, Pel: Peloponnese, PP: Pelion Peninsula, PSF: Pelion-Skopelos Fault, S: Samothraki, SiG: Sigitikos Gulf, SiP: Sithonia Peninsula, Sk: Skyros, SKF: Skyros Fault, SpA: Sporades Archipelago, Th: Thasos, ThG: Thermaikos Gulf. General topography and bathymetry from SRTM30 (Becker et al., 2009) and high resolution bathymetry (250m) from Sakellariou and Tsampouraki-Kraounaki (2016).

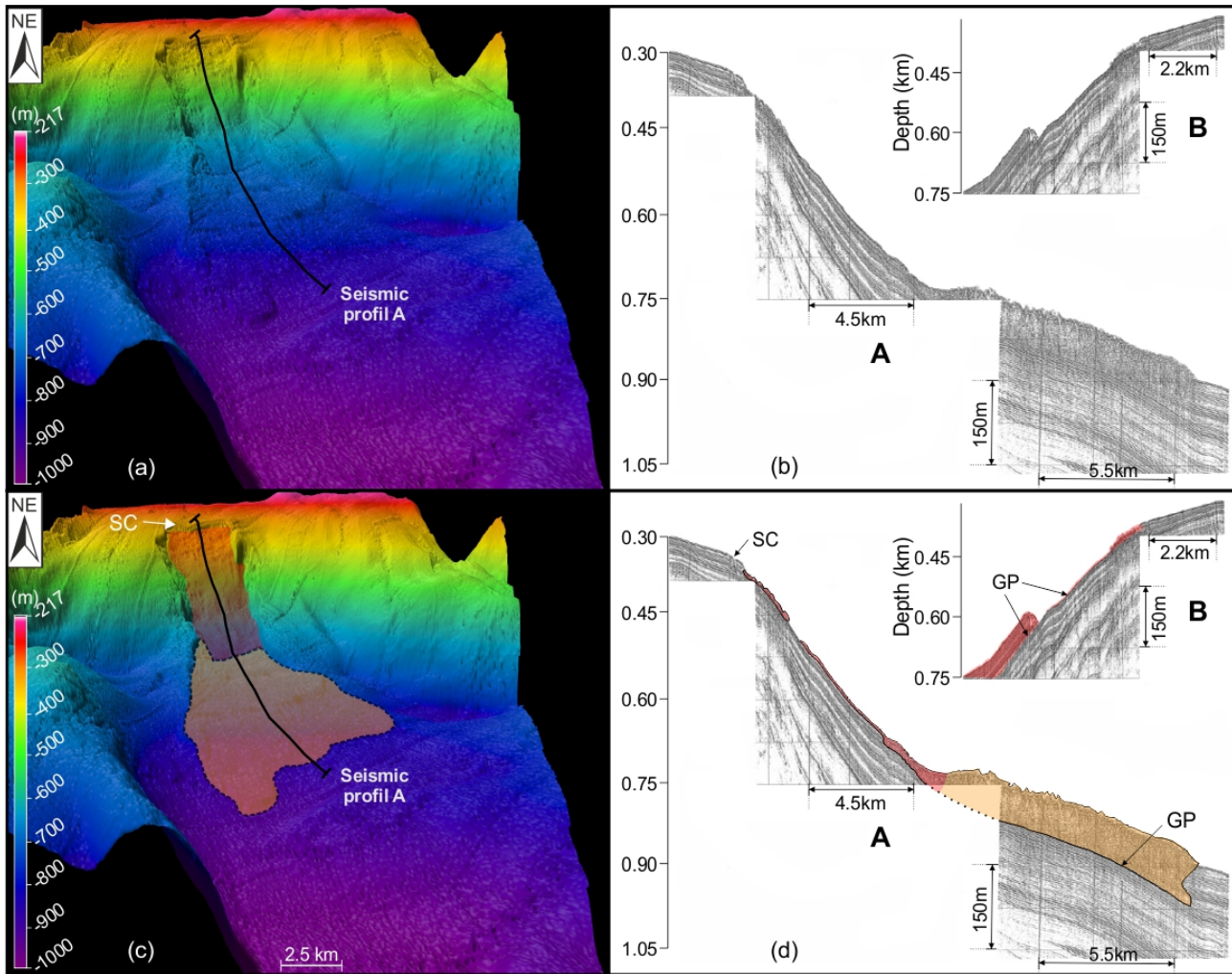


Figure 12. Features of the Thasos submarine landslide. In red, the first unit, in orange, the second unit. (a): 3-D view of the actual bathymetry of the Thasos landslide. (b): raw seismic profiles from Lykousis et al. (2002): (A) Downslope air-gun sub-bottom profile indicated on (a) and (B) details of the seismic profile along the major glide zone. (c): interpretation of the 3-D bathymetry : in red the area where the deposit is thin or non-existent in the upper part of the slide; in orange the area where the deposit is thick (marked on the bathymetry by a hummocky facies and in the seismic profile by chaotic and hyperbolic reflectors); SC: slide scarp. (d): Interpretation of seismic profiles with the same convention as in (c), GP: glide plane. (b) and (d): modified after Lykousis et al. (2002).

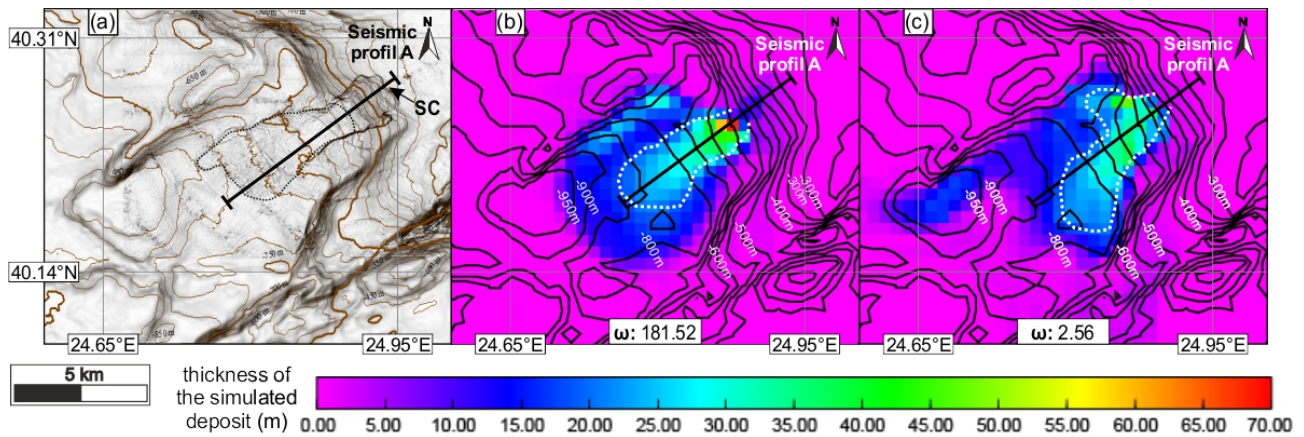


Figure 13. Numerical reconstruction of the final position of the slide for the two credible scenarios. (a): Multibeam bathymetry of the slide. Black dotted line corresponds to the limit of the slide deposit (in orange on Fig.12). (b): position of the slide’s deposit for the first credible scenario. White dotted line highlights the main transport deposit (above 20 m thick). The resolution of the seismic profile is not enough to track the mass transport deposit thin than 20 m thick. (c): position of the slide’s deposit for the second credible scenario with the same convention as in (b). ω is a coherence index. The higher this index is, the closer the simulation is to the observable data. This index is defined with normalized inverse distance weighting (Appendix A). SC: slide scarp.

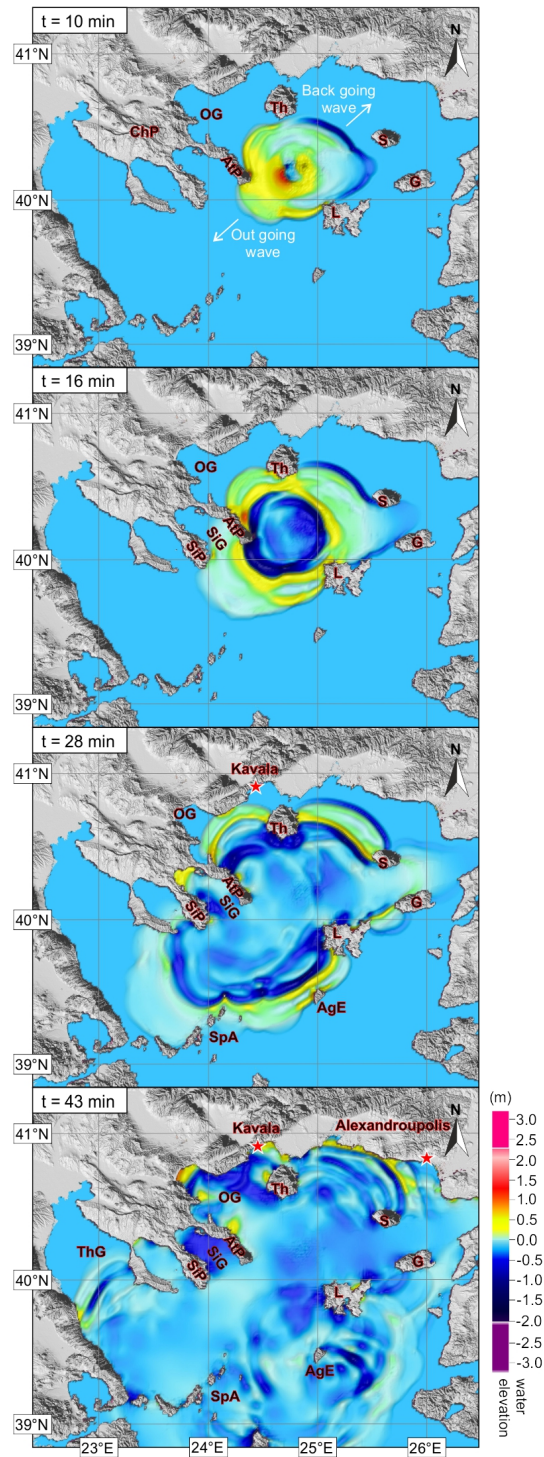


Figure 14. Tsunami propagation in the case of the first credible scenario. (e_w of 10^{-3} and a basal friction angle of 1° ; Table. 11). AgE: Agios Efrstratios, AtP: Athos Peninsula, G: Gokceada, L: Lemnos, OG: Orfani Gulf, S: Samothraki, SiG: Sigitikos Gulf, SiP: Sithonia Peninsula, SpA: Sporades Archipelago, Th: Thasos, ThG: Thermaikos Gulf.

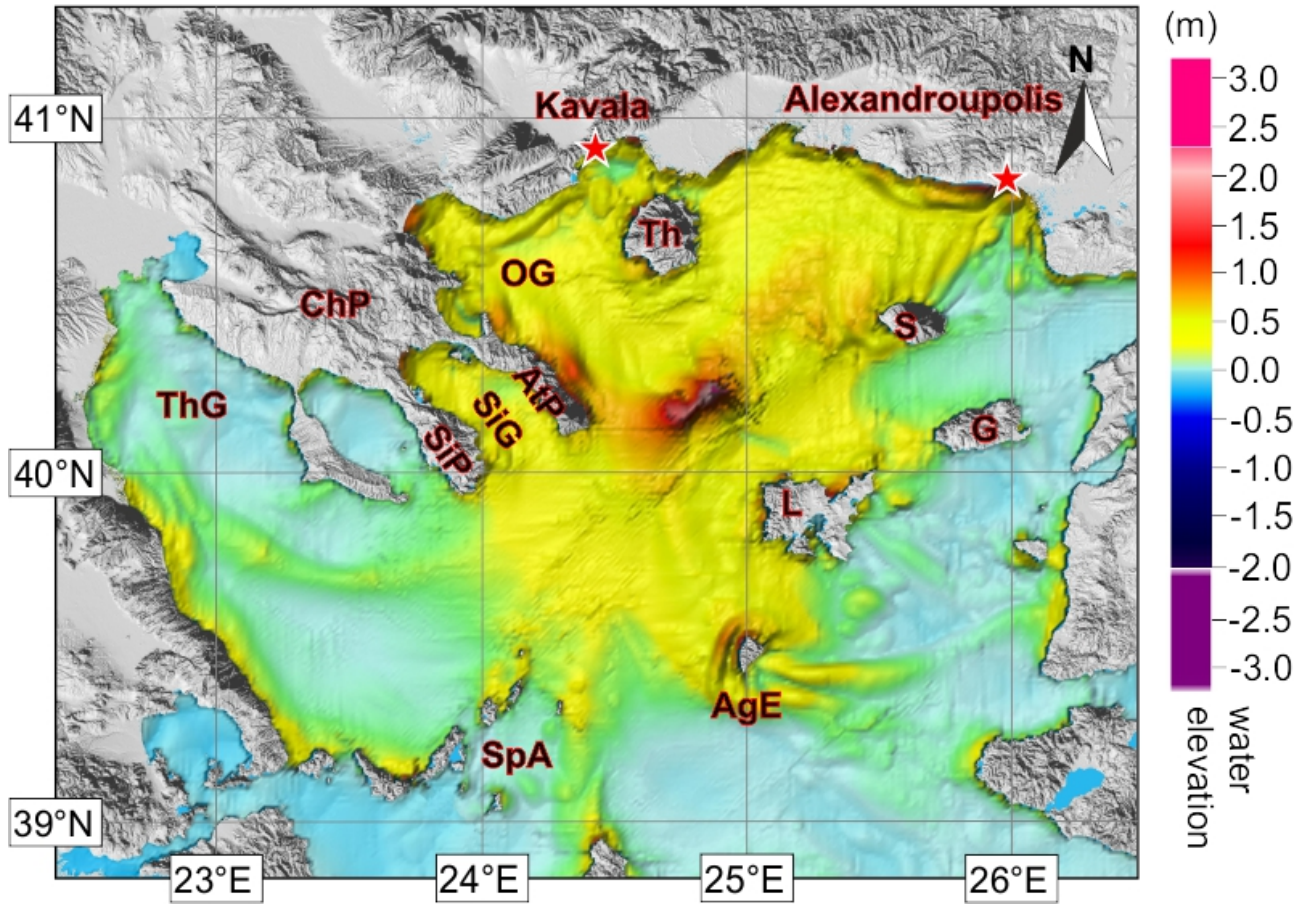


Figure 15. Figure of the maximum water elevation of the tsunami for the first credible scenario (Table. 11). AgE: Agios Efstratios, AtP: Athos Peninsula, G: Gokceada, L: Lemnos, OG: Orfani Gulf, S: Samothraki, SiG: Sigitikos Gulf, SiP: Sithonia Peninsula, SpA: Sporades Archipelago, Th: Thasos, ThG: Thermaikos Gulf.

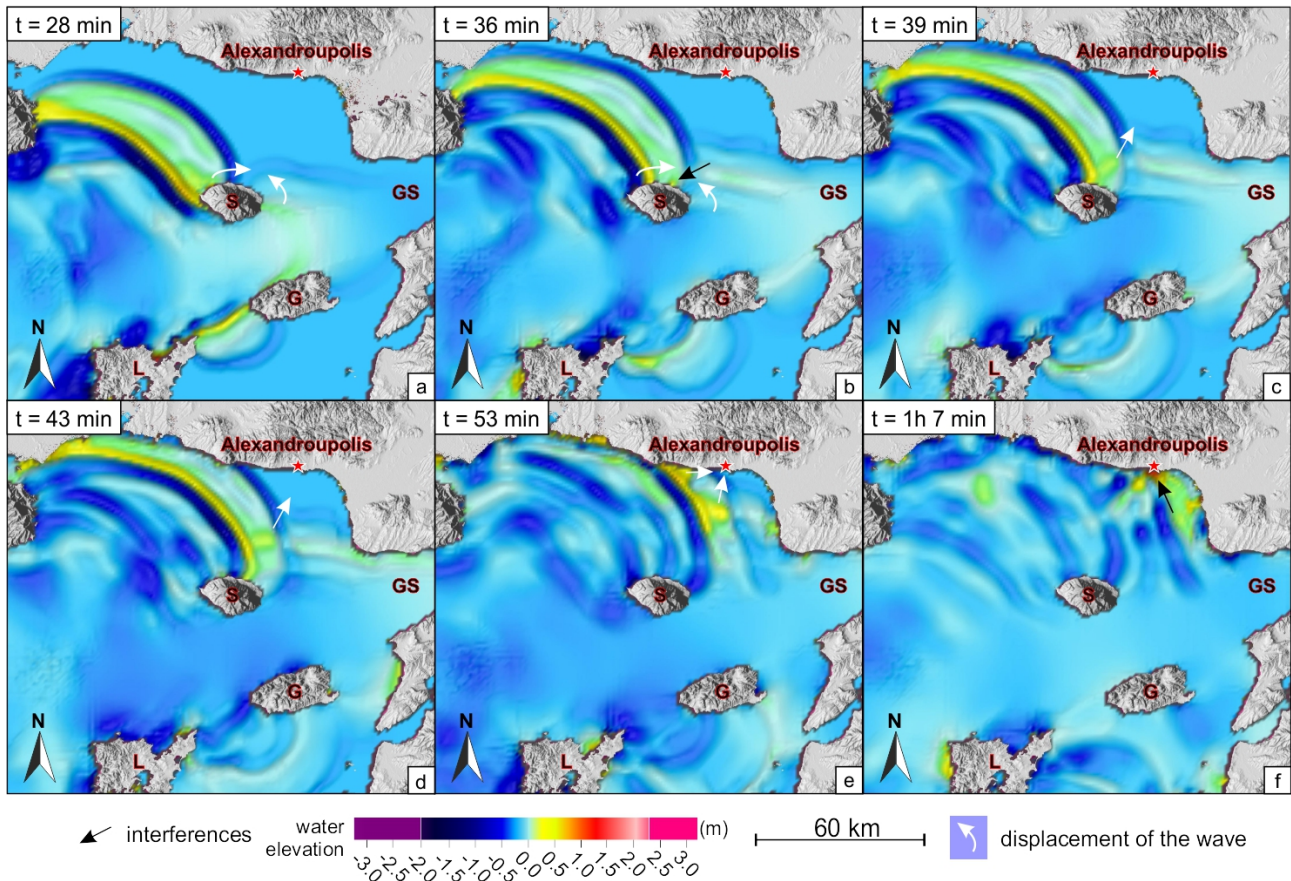


Figure 16. Tsunami propagation in the NE of Aegean Sea : illustration of a complex system of amplification by interferences for the first credible scenario (Table. 11). GS: Gulf of Saros G: Gokceada, L: Lemnos, OG: Orfani Gulf, S: Samothraki. (a): arrival in the South of Samothraki of wavefront, (b): rotation of the wavefront around Samothraki and development of constructive interferences in the North of the island., (c): recess of the wavefront of the island, (d): migration to the North for the new wavefront, (e): arrival of a other front by the west, (f): constructive interferences in front of Alexandroupolis and formation of a wave of 1.65 m high.

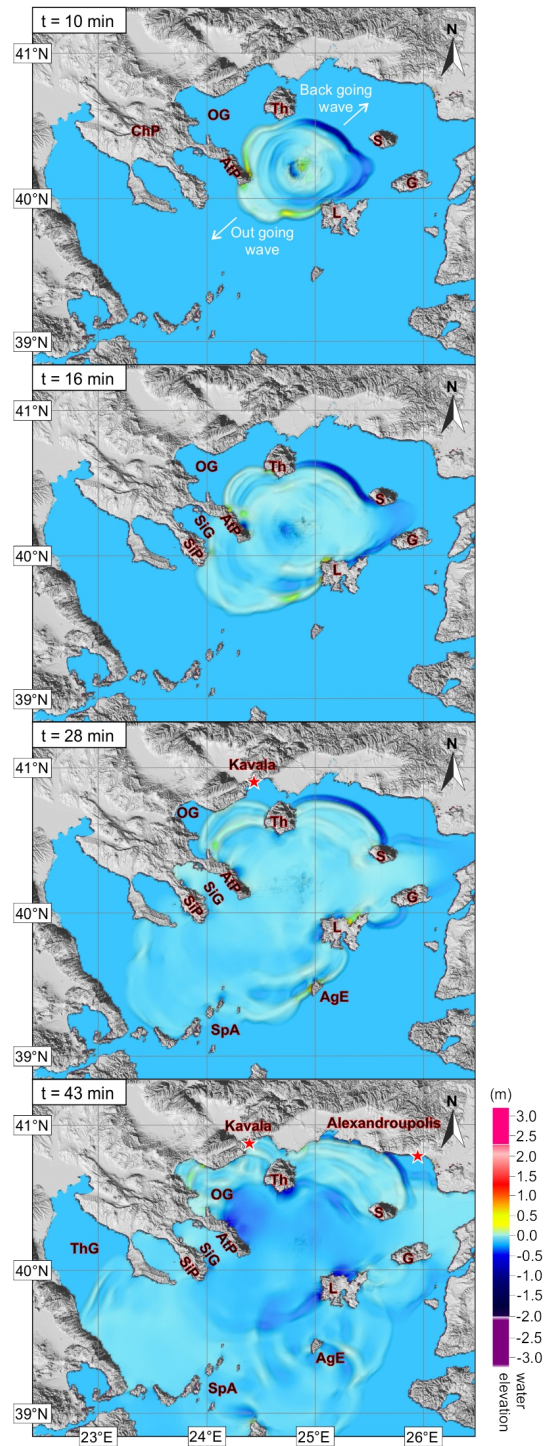


Figure 17. Tsunami propagation in the case of the second credible scenario. (e_w of $5 \cdot 10^{-4}$ and a basal friction angle of 1.5° ; Table. 11). AgE: Agios Efstratios, AtP: Athos Peninsula, G: Gokceada, L: Lemnos, OG: Orfani Gulf, S: Samothraki, SiG: Sigitikos Gulf, SiP: Sithonia Peninsula, SpA: Sporades Archipelago, Th: Thasos, ThG: Thermaikos Gulf.

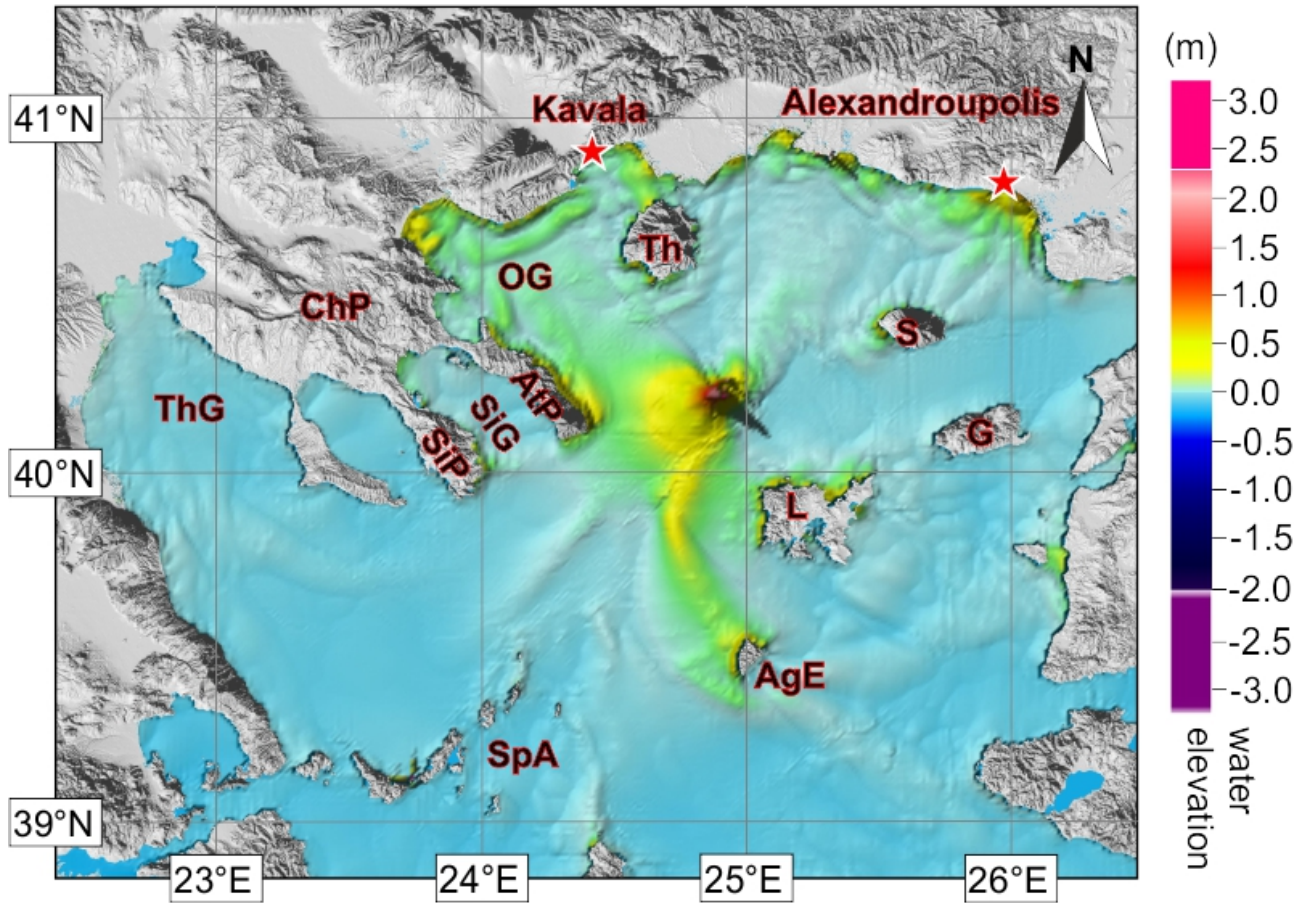


Figure 18. Figure of the maximum water elevation of the tsunami for the second credible scenario (Table. 11). AgE: Agios Efstratios, AtP: Athos Peninsula, G: Gokceada, L: Lemnos, OG: Orfani Gulf, S: Samothraki, SiG: Sigitikos Gulf, SiP: Sithonia Peninsula, SpA: Sporades Archipelago, Th: Thasos, ThG: Thermaikos Gulf.

Table 11. Table of key parameters used for produced the 2 most credible scenrios. Vi: Initial volume, TRUN: total simulated time, TSLISTOP: slide is stopped at tslistop, PHIBAS: basal friction angle, e_w : water entrainment coefficient, Vf: final volume of the slide.

Credible scenarios	Vi(km^3)	TRUN(s)	TSLPISTOP(s)	PHIBAS($^\circ$)	e_w	Vf(km^3)
1 st scenario	1.8511	7200	600	1.0	$1 \cdot 10^{-3}$	3.6938
2 nd scenario	1.8511	7200	1700	1.5	$5 \cdot 10^{-4}$	4.1103

Table 12. Table of maximum elevation (cm) of the water level for 10 places where the tsunami was amplified. Top: Above the marine landslide, AgE: Agios Efstratios, AtP: Athos Peninsula, L: Lemnos (Gulf of Pournias), OG: Orfani Gulf, SpA: Sporades Archipelago, Th: Thasos.

Credible scenarios	Top	Th	L	AgE	SpA	AtP	OG	Kavala	Alexandroupolis	Turkey
1 st scenario	360	115	140	145	145	145	120	65	165	75
2 nd scenario	470	75	105	110	80	120	40	25	60	40